

Author Manuscript

This is the author manuscript accepted for publication and has undergone full peer review but has not been through the copyediting, typesetting, pagination and proofreading process, which may lead to differences between this version and the [Version of Record](#). Please cite this article as [doi: 10.1111/ANZS.12318](https://doi.org/10.1111/ANZS.12318)

This article is protected by copyright. All rights reserved

Globally intensity-reweighted estimators for K - and pair correlation functions

Thomas Shaw¹, Jesper Møller^{2*} and Rasmus Plenge Waagepetersen³

University of Michigan and Aalborg University

Summary

We introduce new estimators of the inhomogeneous K -function and the pair correlation function of a spatial point process as well as the cross K -function and the cross pair correlation function of a bivariate spatial point process under the assumption of second-order intensity-reweighted stationarity. These estimators rely on a ‘global’ normalisation factor which depends on an aggregation of the intensity function, whilst the existing estimators depend ‘locally’ on the intensity function at the individual observed points. The advantages of our new global estimators over the existing local estimators are demonstrated by theoretical considerations and a simulation study.

Key words: inhomogeneous K -function; intensity function; kernel estimation; pair correlation function; second-order intensity-reweighted stationarity; spatial point process

1. Introduction

Functional summary statistics like the nearest-neighbour-, the empty space-, and Ripley’s K -function have a long history in statistics for spatial point processes (Møller & Waagepetersen 2004; Illian et al. 2008; Chiu et al. 2013). For many years the theory of these functional summary statistics was confined to the case of stationary point processes with consequently constant intensity functions. The paper Baddeley, Møller & Waagepetersen (2000) was therefore a big step forward since it relaxed substantially the assumption of stationarity in case of the K -function and the closely related pair correlation function.

Baddeley, Møller & Waagepetersen (2000) introduced the notion of second-order intensity-reweighted stationarity (*soirs*) for a spatial point process. When the pair correlation

*Author to whom correspondence should be addressed.

¹ Applied Physics Program, University of Michigan, 1425 Randall Laboratory, 450 Church St, Ann Arbor, MI, 48109, USA

² Department of Mathematical Sciences, Aalborg University, Skjernvej 4A, 9220 Aalborg Ø, Denmark, Email: jm@math.aau.dk

³ Department of Mathematical Sciences, Aalborg University, Skjernvej 4A, 9220 Aalborg Ø, Denmark

Acknowledgment. The first author was supported by grants from the U.S. National Science Foundation (MCB1552439) and National Institutes of Health (R01GM129347) and he thanks his advisor Dr. Sarah Veatch for her support. The last two authors were supported by the ‘Danish Council for Independent Research — Natural Sciences’ grant DFF – 7014-00074 ‘Statistics for point processes in space and beyond’, and by the ‘Centre for Stochastic Geometry and Advanced Bioimaging’ funded by grant 8721 from the Villum Foundation.

17 function g exists for the point process, soirs is equivalent to g being translation invariant.
18 However, the intensity function does not need to be constant, which is a great improvement
19 compared to assuming stationarity, see e.g. Møller & Waagepetersen (2007). When the point
20 process is soirs, Baddeley, Møller & Waagepetersen (2000) introduced a generalisation of
21 Ripley's K -function, the so-called inhomogeneous K -function, which is based on the idea of
22 intensity-reweighting the points of the spatial point process, and they discussed its estimation.
23 The inhomogeneous K -function has found applications in a very large number of applied
24 papers and has also been generalised e.g. to the case of space-time point processes (Gabriel
25 & Diggle 2009) and to point processes on spheres (Lawrence et al. 2016; Møller & Rubak
26 2016). Moreover, van Lieshout (2011) used the idea of intensity-reweighting to generalise the
27 so-called J -function to the case of inhomogeneous point processes.

28 A generic problem in spatial statistics, when just one realisation of a spatial process is
29 available, is to separate variation due to random interactions from variation due to a non-
30 constant intensity or mean function. In general, if an informed choice of a parsimonious
31 intensity function model is available for a point process, the intensity function can be
32 estimated consistently. Consistent estimation of the inhomogeneous K -function is then
33 also possible when the consistent intensity function estimate is used to reweight the point
34 process, see e.g. Waagepetersen & Guan (2009) in case of regression models for the intensity
35 function. When a parsimonious model is not available, one may resort to non-parametric
36 kernel estimation of the intensity function as considered initially in Baddeley, Møller
37 & Waagepetersen (2000). However, kernel estimators are not consistent for the intensity
38 function and they are strongly upwards biased when evaluated at the observed points. This
39 implies strong bias of the resulting inhomogeneous K -function estimators when the kernel
40 estimators are plugged in for the true intensity.

41 In this paper, we introduce a new approach to non-parametric estimation of the
42 (inhomogeneous) K and g -functions for a spatial point process, or of the cross K -function
43 and the cross pair correlation for a bivariate spatial point process, assuming soirs in both
44 cases. This formalises an approach that was used by Stone et al. (2017) to estimate space-
45 time cross pair correlation functions in live-cell single molecule localisation microscopy
46 experiments with spatially varying localisation probabilities. In the univariate case, our new
47 as well as the existing estimators are given by a sum over all distinct points x and y from
48 an observed point pattern. For the new estimators, each term in the sum depends on an
49 aggregation of the intensity function through a 'global' normalization factor $\gamma(y - x)$ instead
50 of depending 'locally' on the intensity function at x and at y as for the existing estimators
51 (a similar remark applies in the bivariate case). Intuitively one may expect this to mitigate
52 the problem of using biased kernel estimators of the intensity function in connection to non-
53 parametric estimation of the K -function or pair correlation function. Moreover, to reduce bias

54 when using a non-parametric kernel estimator of γ , we propose a ‘leave-out’ modification
 55 of our γ estimator. Our simulation study shows that our new globally intensity reweighted
 56 estimators are superior to the existing local estimators in terms of bias and estimation variance
 57 regardless of whether the intensity function is estimated parametrically or non-parametrically.

58 The remainder of the paper is organised as follows. Some background on spatial point
 59 processes and notational details are provided in Section 2. Section 3 introduces our global
 60 estimator for the K -function or the cross K -function, discusses modifications to account
 61 for isotropy, and compares with the existing local estimators. Section 4 is similar but for
 62 our new global estimator of the g -function or cross pair correlation function. Section 5
 63 describes sources of bias in the local and global estimators when kernel estimators are used,
 64 and modifications to reduce bias. In Section 6, the global and local estimators of K and g
 65 are compared in a simulation study. Possible extensions are discussed in Section 7. Finally,
 66 Section 8 contains some concluding remarks.

67 2. Preliminaries

68 We consider the usual setting for a spatial point process X defined on the d -dimensional
 69 Euclidean space \mathbb{R}^d , that is, X is a random locally finite subset of \mathbb{R}^d . This means that
 70 the number of points from X falling in A , denoted $N(A)$, is almost surely finite for any
 71 bounded subset A of \mathbb{R}^d . For further details we refer to Møller & Waagepetersen (2004). In
 72 our examples, $d = 2$.

73 For any integer $n \geq 1$, we say that X has n 'th order intensity function $\rho^{(n)} : (\mathbb{R}^d)^n \mapsto$
 74 $[0, \infty)$ if for any disjoint bounded Borel sets $A_1, \dots, A_n \subset \mathbb{R}^d$,

$$E\{N(A_1) \cdots N(A_n)\} = \int_{A_1} \cdots \int_{A_n} \rho^{(n)}(x_1, \dots, x_n) dx_1 \cdots dx_n < \infty.$$

75 By the so-called standard proof we obtain the n 'th order Campbell's formula (see e.g. Møller
 76 & Waagepetersen 2004): for any Borel function $k : (\mathbb{R}^d)^n \mapsto [0, \infty)$,

$$E \sum_{\substack{\neq \\ x_1, \dots, x_n \in X}} k(x_1, \dots, x_n) = \int \cdots \int k(x_1, \dots, x_n) \rho^{(n)}(x_1, \dots, x_n) dx_1 \cdots dx_n,$$

77 which is finite if the left or right hand side is so. Here, \neq over the summation sign means that
 78 x_1, \dots, x_n are pairwise distinct.

79 Throughout this paper, we assume that X has an intensity function ρ and a translation
 80 invariant pair correlation function g . This means that for all $x, y \in \mathbb{R}^d$, $\rho^{(1)}(x) = \rho(x)$
 81 and $\rho^{(2)}(x, y) = \rho(x)\rho(y)g(x, y)$, where $g(x, y) = g_0(x - y)$ with $g_0 : \mathbb{R}^d \mapsto [0, \infty)$ a
 82 symmetric Borel function. If ρ is constant we say that X is (first-order) homogeneous. In

83 particular, if X is stationary, that is, the distribution of X is invariant under translations in
84 \mathbb{R}^d , then ρ is constant and g is translation invariant.

85 Following Baddeley, Møller & Waagepetersen (2000), the translation invariance of g
86 implies that X is second-order intensity reweighted stationary (soirs) and the *inhomogeneous*
87 *K-function* (or just *K-function*) is then given by

$$K(t) := \int_{\|h\| \leq t} g_0(h) \, dh, \quad t \geq 0.$$

88 This is Ripley's *K-function* when X is stationary.

89 Suppose X_1 and X_2 are locally finite point processes on \mathbb{R}^d such that X_i has intensity
90 function ρ_i , $i = 1, 2$, and (X_1, X_2) has a translation invariant *cross pair correlation function*
91 $g_{12}(x_1, x_2) = c(x_1 - x_2)$ for all $x_1, x_2 \in \mathbb{R}^d$. That is, for bounded Borel sets $A_1, A_2 \subset \mathbb{R}^d$
92 and $N_i(A_i)$ denoting the cardinality of $X_i \cap A_i$, $i = 1, 2$, we have

$$\mathbb{E}\{N_1(A_1)N_2(A_2)\} = \int_{A_1} \int_{A_2} \rho_1(x_1)\rho_2(x_2)c(x_1 - x_2) \, dx_1 \, dx_2.$$

93 Then the *cross K-function* is defined by

$$K_{12}(t) := \int_{\|h\| \leq t} c(h) \, dh, \quad t \geq 0.$$

94 In practice X, X_1, X_2 are observed within a bounded window $W \subset \mathbb{R}^d$, and we use
95 the following notation. The translate of W by $x \in \mathbb{R}^d$ is denoted $W_x := \{w + x \mid w \in W\}$.
96 For a Borel set $A \subseteq \mathbb{R}^d$, $\mathbf{1}[x \in A]$ denotes the indicator function which is 1 if $x \in A$ and 0
97 otherwise. The Lebesgue measure of A (or area of A when $d = 2$) is denoted $|A|$, and $\|x\|$ is
98 the usual Euclidean length of $x \in \mathbb{R}^d$.

99 3. Global and local intensity-reweighted estimators for *K-functions*

100 3.1. The case of one spatial point process

101 Considering the setting in Section 2 for the spatial point process X , we define

$$\gamma(h) = \int_{W \cap W_{-h}} \rho(u)\rho(u+h) \, du, \quad h \in \mathbb{R}^d. \quad (1)$$

102 Clearly, γ is symmetric, that is, $\gamma(h) = \gamma(-h)$, for all $h \in \mathbb{R}^d$. We assume that with
 103 probability 1, $\gamma(y - x) > 0$, for all distinct $x, y \in X \cap W$. Then, for $t \geq 0$, we can define

$$\hat{K}_{\text{global}}(t) = \sum_{x, y \in X \cap W}^{\neq} \frac{\mathbf{1}[\|y - x\| \leq t]}{\gamma(y - x)}. \quad (2)$$

If $\gamma(h) > 0$ whenever $\|h\| \leq t$, then $\hat{K}_{\text{global}}(t)$ is an unbiased estimator of $K(t)$. This follows from the second-order Campbell's formula:

$$\begin{aligned} E\hat{K}_{\text{global}}(t) &= \int \int \frac{\mathbf{1}[x \in W, y \in W, \|y - x\| \leq t]}{\gamma(y - x)} \rho(x)\rho(y)g_0(y - x) dx dy \\ &= \int \int \frac{\mathbf{1}[x \in W \cap W_{-h}, \|h\| \leq t]}{\gamma(h)} \rho(x)\rho(x + h)g_0(h) dx dh \\ &= \int_{\|h\| \leq t} \frac{\gamma(h)}{\gamma(h)} g_0(h) dh = K(t). \end{aligned}$$

104 We call \hat{K}_{global} the *global estimator* since it contrasts with one of the estimators
 105 suggested in Baddeley, Møller & Waagepetersen (2000): assuming that almost surely $|W \cap$
 106 $W_{y-x}| > 0$, for all distinct $x, y \in X \cap W$,

$$\hat{K}_{\text{local}}(t) = \sum_{x, y \in X \cap W}^{\neq} \frac{\mathbf{1}[\|y - x\| \leq t]}{\rho(x)\rho(y)|W \cap W_{y-x}|}, \quad (3)$$

107 which we refer to as the *local estimator*. Note that $\hat{K}_{\text{local}}(t)$ is also an unbiased estimator of
 108 $K(t)$ provided $|W \cap W_h| > 0$, for $\|h\| \leq t$. In the homogeneous case,

$$\gamma(h) = \rho^2 |W \cap W_{-h}|,$$

109 whereby $\hat{K}_{\text{global}} = \hat{K}_{\text{local}}$, and in the stationary case, these estimators coincide with the Ohser
 110 & Stoyan (1981) translation estimator.

111 In practice ρ and hence γ must be replaced by estimates. Estimators of ρ and γ and the
 112 bias of these estimators are discussed in Section 5.

113 3.1.1. Modifications to account for isotropy

114 In addition to soirs, it is frequently assumed that the pair correlation function is isotropic
 115 meaning that $g_0(h) = g_1(\|h\|)$ for some Borel function $g_1 : [0, \infty) \mapsto [0, \infty)$. We benefit
 116 from this by integrating over the sphere: for $r > 0$, define

$$\gamma^{\text{iso}}(r) = \int_{\mathbb{S}^{d-1}} \gamma(rs) d\nu_{d-1}(s) / c_d, \quad (4)$$

117 where $\mathbb{S}^{d-1} = \{s \in \mathbb{R}^d \mid \|s\| = 1\}$ denotes the $(d-1)$ -dimensional unit-sphere, ν_{d-1} is the
 118 $(d-1)$ -dimensional surface measure on \mathbb{S}^d , and $\varsigma_d = 2\pi^{d/2}/\Gamma(d/2)$ is the surface area of the
 119 unit sphere \mathbb{S}^{d-1} . Thus $\gamma^{\text{iso}}(r)$ is the mean value of $\gamma(H)$ when H is a uniformly distributed
 120 point on the $(d-1)$ -dimensional sphere of radius r and center at the origin.

121 Assuming that almost surely $\gamma^{\text{iso}}(\|y-x\|) > 0$, for all distinct $x, y \in X \cap W$, this
 122 naturally leads to another global estimator for K when the pair correlation function is
 123 isotropic, namely

$$\hat{K}_{\text{global}}^{\text{iso}}(t) = \sum_{x,y \in X \cap W}^{\neq} \frac{\mathbf{1}[\|y-x\| \leq t]}{\gamma^{\text{iso}}(\|y-x\|)}. \quad (5)$$

That $\hat{K}_{\text{global}}^{\text{iso}}$ is unbiased follows from a similar derivation as for \hat{K}_{global} : for any $t \geq 0$ such
 that $\gamma^{\text{iso}}(r) > 0$ whenever $r \leq t$,

$$\begin{aligned} \mathbb{E} \hat{K}_{\text{global}}^{\text{iso}}(t) &= \int_{\|h\| \leq t} \frac{\gamma(h)}{\gamma^{\text{iso}}(\|h\|)} g_0(h) \, dh \\ &= \int_0^t g_1(r) r^{d-1} \int_{\mathbb{S}^{d-1}} \frac{\gamma(rs)}{\gamma^{\text{iso}}(r)} \, d\nu_{d-1}(s) \, dr \end{aligned} \quad (6)$$

$$\begin{aligned} &= \int_0^t g_1(r) \varsigma_d r^{d-1} \, dr \\ &= \int_{\|h\| \leq t} g_1(\|h\|) \, dh = K(t), \end{aligned} \quad (7)$$

124 where (6) and (7) employ changes of variables to and from polar coordinates, respectively.

125 When X is homogeneous, (5) coincides with the Ohser & Stoyan (1981) isotropic
 126 estimator. A local estimator of this form can also be defined:

$$\hat{K}_{\text{local}}^{\text{iso}}(t) = \sum_{x,y \in X \cap W} \frac{\mathbf{1}[\|y-x\| \leq t]}{\rho(x)\rho(y)a_W(\|y-x\|)}, \quad (8)$$

127 where

$$a_W(r) = \int_{\mathbb{S}^{d-1}} |W \cap W_{-rs}| \, d\nu_{d-1}(s) / \varsigma_d \quad (9)$$

128 is an isotropized edge correction factor, and where it is assumed that almost surely $a_W(\|y-x\|) > 0$,
 129 for all distinct $x, y \in X \cap W$. The local estimator is unbiased when $a_W(r) > 0$, for
 130 all $r \leq t$.

131 3.1.2. Comparison of local and global estimators

132 The global and local estimators (2) and (3) differ in the relative weighting of distinct
 133 points $x, y \in X \cap W$. Namely, \hat{K}_{local} weights pairs x, y from low-density areas more
 134 strongly than those from high-density areas, whilst for \hat{K}_{global} , the weight only depends

135 on the difference $y - x$. Theoretical expressions for the variances of the global and local K -
 136 function estimators are very complicated, not least when the intensity function is replaced by
 137 an estimate. This makes it difficult to make a general theoretical comparison of the estimators
 138 in terms of their variances. However, under some simplifying assumptions insight can be
 139 gained as explained in the following.

Consider a quadratic observation window W of sidelength nm . Then W is a disjoint union of n^2 quadrats W_1, \dots, W_{n^2} each of sidelength m . Assume that the intensity function is constant and equal to ρ_i within each W_i , with ρ naturally estimated by $\hat{\rho}(u) = \hat{\rho}_i = N(W_i)/m^2$, for $u \in W_i$. For fixed t and large m , when ρ is replaced by its estimator $\hat{\rho}$, we can now approximate the local estimator:

$$\begin{aligned} \hat{K}_{\text{local}}(t) &= \sum_{u,v \in X \cap W}^{\neq} \frac{\mathbf{1}[\|u-v\| \leq t]}{\hat{\rho}(u)\hat{\rho}(v)|W \cap W_{u-v}|} \simeq \sum_{i=1}^{n^2} \sum_{u,v \in X \cap W_i}^{\neq} \frac{\mathbf{1}[\|u-v\| \leq t]}{\hat{\rho}_i^2 |W \cap W_{u-v}|} \\ &\simeq \sum_{i=1}^{n^2} \sum_{u,v \in X \cap W_i}^{\neq} \frac{\mathbf{1}[\|u-v\| \leq t]}{\hat{\rho}_i^2 |W_i \cap (W_i)_{u-v}| n^2} = \frac{1}{n^2} \sum_{i=1}^{n^2} \hat{K}_{i,\text{local}}(t). \end{aligned}$$

140 where $\hat{K}_{i,\text{local}}$ is the local estimator based on $X \cap W_i$. We use here \simeq in a rather loose sense,
 141 meaning that asymptotically, as m tends to infinity, the difference between the two quantities
 142 on each side of \simeq tends to zero in a suitable sense (e.g. in mean square) under appropriate
 143 regularity conditions. The first approximation above follows because contributions from $u \in$
 144 X_i and $v \in X_j$, $i \neq j$, are negligible for fixed t and m large, and the second approximation
 145 is justified since for $\|h\| \leq t$, $|W|/|W \cap W_h|$ and $|W_i|/|W_i \cap (W_i)_h|$ will tend to 1 as m
 146 increases. Following similar steps, we obtain for the global estimator,

$$\hat{K}_{\text{global}}(t) \simeq \sum_{i=1}^{n^2} \hat{K}_{i,\text{local}}(t) \frac{\hat{\rho}_i^2}{\sum_{l=1}^{n^2} \hat{\rho}_l^2}.$$

147 Suppose X is a Poisson process. Note that $\hat{K}_{\text{local}}(t)$ is an equally weighted average
 148 of the $\hat{K}_{i,\text{local}}(t)$, but since the $\hat{K}_{i,\text{local}}(t)$ are independent, the optimal weighted average is
 149 obtained with weights inversely proportional to the variances of the $\hat{K}_{i,\text{local}}(t)$. For large
 150 m , the variance of $\hat{K}_{i,\text{local}}(t)$ is well approximated by $2\pi t^2/(\rho_i^2 m^2)$ (Ripley 1988; Lang &
 151 Marcon 2013) and the optimal weights w_i are thus proportional to ρ_i^2 . Our global estimator
 152 is obtained from the optimal weighted average by replacing the optimal weights by natural
 153 consistent estimates. Hence one may anticipate that the global estimator has smaller variance
 154 than the local estimator. In a small-scale simulation study this was indeed the case, and the
 155 global estimator with (random) weights proportional to $\hat{\rho}_i^2$ even had slightly smaller variance
 156 than when the optimal fixed weights $w_i \propto \rho_i^2$ were used.

157 3.2. The case of two spatial point processes

158 For two spatial point processes X_1 and X_2 observed on the same observation window
 159 W (cf. Section 2), we define the following global estimator for the cross K -function: for
 160 $t \geq 0$,

$$\hat{K}_{12,\text{global}}(t) = \sum_{x \in X_1 \cap W, y \in X_2 \cap W} \frac{\mathbf{1}[\|y - x\| \leq t]}{\gamma_{12}(y - x)} \quad (10)$$

161 where

$$\gamma_{12}(h) = \int_{W \cap W_{-h}} \rho_1(u) \rho_2(u + h) du$$

162 and it assumed that almost surely $\gamma_{12}(y - x) > 0$, for all $x \in X_1 \cap W$ and $y \in X_2 \cap W$. It
 163 is straightforwardly verified that $\hat{K}_{12,\text{global}}(t)$ is unbiased for any $t \geq 0$ such that $\gamma_{12}(h) > 0$
 164 whenever $\|h\| \leq t$.

165 The corresponding local estimator is

$$\hat{K}_{12,\text{local}}(t) = \sum_{x \in X_1 \cap W, y \in X_2 \cap W} \frac{\mathbf{1}[\|y - x\| \leq t]}{\rho_1(x) \rho_2(y) |W \cap W_{y-x}|}, \quad (11)$$

166 assuming that almost surely $|W \cap W_{y-x}| > 0$ for $x \in X_1 \cap W$ and $y \in X_2 \cap W$. The local
 167 estimator is unbiased when $|W \cap W_h| > 0$ for $\|h\| \leq t$.

168 Interchanging X_1 and X_2 does not affect (10): $\hat{K}_{12,\text{global}}(t) = \hat{K}_{21,\text{global}}(t)$ when
 169 $\hat{K}_{21,\text{global}}(t)$ is defined as in (10) with γ_{12} replaced by

$$\gamma_{21}(h) = \int_{W \cap W_{-h}} \rho_1(u + h) \rho_2(u) du.$$

170 This follows since by a change of variable, γ_{12} is symmetric, $\gamma_{21}(h) = \gamma_{12}(-h) = \gamma_{12}(h)$.

171 When the cross pair correlation function $c(h)$ is also isotropic, additional unbiased
 172 estimators of K_{12} are readily obtained in the same way as for the one point process case.

173 Thus, defining

$$\gamma_{12}^{\text{iso}}(r) = \int_{\mathbb{S}^{d-1}} \gamma_{12}(rs) d\nu_{d-1}(s) / \varsigma_d, \quad r \geq 0, \quad (12)$$

174 and assuming that almost surely $\gamma_{12}^{\text{iso}}(\|y - x\|) > 0$ for $x \in X_1 \cap W$ and $y \in X_2$, we define
 175 an isotropic global estimator by

$$\hat{K}_{12,\text{global}}^{\text{iso}}(t) = \sum_{x \in X_1 \cap W, y \in X_2 \cap W}^{\neq} \frac{\mathbf{1}[\|y - x\| \leq t]}{\gamma_{12}^{\text{iso}}(\|y - x\|)}. \quad (13)$$

176 This is easily seen to be unbiased when $\gamma_{12}^{\text{iso}}(r) > 0$ for $r \leq t$. Finally, the isotropic local
177 estimator is

$$\hat{K}_{12,\text{local}}^{\text{iso}}(t) = \sum_{x \in X_1 \cap W, y \in X_2 \cap W}^{\neq} \frac{\mathbf{1}[\|y - x\| \leq t]}{\rho_1(x)\rho_2(y)a_W(\|y - x\|)}, \quad (14)$$

178 with $a_W(r)$ as defined in Section 3.1.1, and it becomes unbiased if $a_W(r) > 0$, for all $r \leq t$.

179 4. Global and local intensity-reweighted estimators for pair correlation functions

180 4.1. The case of one spatial point process

181 Considering again the setting in Section 2 for the spatial point process X , this section
182 introduces global and local estimators for the translation invariant pair correlation function
183 given by g_0 . Note that it may be easier to interpret g_0 than K , but non-parametric kernel
184 estimation of g_0 involves the choice of a bandwidth.

Let $\kappa_b : \mathbb{R}^d \mapsto [0, \infty)$ be a (normalised) kernel with bandwidth $b > 0$, that is, $\kappa_b(h) = \kappa_1(h/b)/b^d$, for all $h \in \mathbb{R}^d$, where κ_1 is a probability density function. We assume that κ_1 has support centered in the origin and contained in $[-k, k]^d$ for some $k > 0$; e.g. κ_1 could be a standard d -dimensional normal density truncated to $[-k, k]^d$ (this choice is convenient when W is rectangular with sides parallel to the usual axes in \mathbb{R}^d). Note that the bounded support of κ_b shrinks to $\{0\}$ when b tends to zero. Then, for $h \in \mathbb{R}^d$,

$$\begin{aligned} \text{E} \sum_{x, y \in X \cap W}^{\neq} \kappa_b(h - (y - x)) \\ &= \int_W \int_W \kappa_b(h - (y - x)) \rho(x) \rho(y) g_0(y - x) \, dx \, dy \end{aligned} \quad (15)$$

$$\begin{aligned} &= \int_W \left\{ \int_{W_{-h-x}} \kappa_b(-z) \rho(x) \rho(x + h + z) g_0(h + z) \, dz \right\} dx \\ &\simeq g_0(h) \int_W \rho(x) \left\{ \int_{W_{-h-x}} \kappa_b(-z) \rho(x + h + z) \, dz \right\} dx \end{aligned} \quad (16)$$

$$\simeq g_0(h) \gamma(h) \quad (17)$$

185 where $\gamma(h)$ is defined in (1). Here, (15) follows from the second-order Campbell's formula
186 and \simeq in (16) and (17) means that the difference between the quantities on each side of \simeq
187 converges to zero as the bandwidth b tends to zero, under appropriate continuity conditions
188 on $\rho(\cdot)$ and $g_0(\cdot)$. The expression (16) is expected to be more accurate but (17) is simpler to
189 compute.

From (17) we conclude that $g_0(h)$ can be estimated by the following *global estimator*,

$$\hat{g}_{\text{global}}(h) = \sum_{x,y \in X \cap W}^{\neq} \kappa_b(h - (y - x)) / \gamma(h),$$

provided $\gamma(h) > 0$. This contrasts with the *local estimator*

$$\hat{g}_{\text{local}}(h) = \sum_{x,y \in X \cap W}^{\neq} \kappa_b(h - (y - x)) / \{\rho(x)\rho(y) |W \cap W_{x-y}|\},$$

190 which is analogous to the estimator suggested in Baddeley, Møller & Waagepetersen (2000)
191 for an isotropic pair correlation function, see also Section 4.1.1.

192 4.1.1. Modifications to account for isotropy

193 For isotropic point processes as defined in Section 3.1.1, the global pair correlation
194 function estimator may be modified to estimate the isotropic pair correlation function given
195 by g_1 : for $r > 0$ such that $\gamma^{\text{iso}}(r) > 0$, define

$$\hat{g}_{\text{global}}^{\text{iso}}(r) = \frac{1}{s_d r^{d-1}} \sum_{x,y \in X \cap W}^{\neq} \tilde{\kappa}_b(r - \|x - y\|) / \gamma^{\text{iso}}(r), \quad (18)$$

where for $b > 0$, $\tilde{\kappa}_b(t) = \tilde{\kappa}_1(t/b)/b$, $t \in \mathbb{R}$, for a probability density $\tilde{\kappa}_1 : \mathbb{R} \mapsto [0, \infty)$ with support centered at 0 and contained in the interval $[-k, k]$ for some constant $k > 0$, and where $\gamma^{\text{iso}}(r)$ is defined in (4). This definition is motivated by the following derivation:

$$\begin{aligned} \text{E} \sum_{x,y \in X \cap W}^{\neq} \tilde{\kappa}_b(r - \|y - x\|) \\ = \int_W \int_W \tilde{\kappa}_b(r - \|y - x\|) \rho(x)\rho(y) g_1(\|y - x\|) dy dx \end{aligned} \quad (19)$$

$$= \int_W \left\{ \int_0^\infty \tilde{\kappa}_b(r - \xi) g_1(\xi) \xi^{d-1} \int_{\mathbb{S}^{d-1}} \rho(x)\rho(x + \xi s) \mathbf{1}[x + \xi s \in W] d\nu_{d-1}(s) d\xi \right\} dx \quad (20)$$

$$\simeq g_1(r) s_d \gamma^{\text{iso}}(r) r^{d-1} \int_0^\infty \tilde{\kappa}_b(r - \xi) d\xi \quad (21)$$

$$\simeq g_1(r) s_d \gamma^{\text{iso}}(r) r^{d-1}, \quad (22)$$

196 using the second-order Cambell formula in (19), a ‘shift to polar coordinates’ in (20), the
197 assumption that b is small in (21), and that the kernel is a probability density function in (22).

198 Note regarding (22) that

$$\int_0^\infty \tilde{\kappa}_b(r - \xi) \, d\xi = \int_{-\infty}^r \tilde{\kappa}_b(\xi) \, d\xi$$

199 which is not 1 in general. Since $\tilde{\kappa}_b(\xi) = 0$ for $\xi \notin [-bk, bk]$, the integral is 1 if $bk < r$. From
200 (22) we obtain (18).

201 In the isotropic case the most commonly used local estimators (Baddeley, Møller &
202 Waagepetersen 2000) are

$$\hat{g}_{\text{local}}^{\text{iso}}(r) = \frac{1}{s_d r^{d-1}} \sum_{x,y \in X \cap W}^{\neq} \frac{\tilde{\kappa}_b(r - \|y - x\|)}{\rho(x)\rho(y)|W \cap W_{x-y}|}$$

203 and

$$\hat{g}_{\text{local}}^{\text{iso}}(r) = \frac{1}{s_d} \sum_{x,y \in X \cap W}^{\neq} \frac{\tilde{\kappa}_b(r - \|y - x\|)}{\rho(x)\rho(y)|W \cap W_{x-y}|\|y - x\|^{d-1}},$$

204 assuming that almost surely $|W \cap W_{x-y}| > 0$ for distinct $x, y \in X \cap W$. These estimators
205 suffer from strong positive respectively negative bias for values of r close to 0.

206 4.2. Two point processes

A similar derivation is possible for the cross pair correlation function of a bivariate point process (X_1, X_2) , yielding similar global and local estimators of $c(h)$: for $\gamma_{12}(h) > 0$,

$$\hat{c}_{\text{global}}(h) = \sum_{x \in X_1 \cap W, y \in X_2 \cap W} \kappa_b(h - (y - x)) / \gamma_{12}(h);$$

for $\gamma_{12}^{\text{iso}}(r) > 0$,

$$\hat{c}_{\text{global}}^{\text{iso}}(r) = \frac{1}{s_d r^{d-1}} \sum_{x \in X_1 \cap W, y \in X_2 \cap W} \tilde{\kappa}_b(r - \|y - x\|) / \gamma_{12}^{\text{iso}}(r);$$

and for $|W \cap W_{x-y}| > 0$ almost surely when $x \in X_1 \cap W$ and $y \in X_2 \cap W$,

$$\hat{c}_{\text{local}}(h) = \sum_{x \in X_1 \cap W, y \in X_2 \cap W} \kappa_b(h - (y - x)) / \{\rho_1(x)\rho_2(y) |W \cap W_{x-y}|\}$$

and

$$\hat{c}_{\text{local}}^{\text{iso}}(r) = \frac{1}{s_d r^{d-1}} \sum_{x \in X_1 \cap W, y \in X_2 \cap W} \frac{\tilde{\kappa}_b(r - \|y - x\|)}{\rho_1(x)\rho_2(y)|W \cap W_{x-y}|}.$$

Also an intermediate estimator is possible, with the intensity weighting for one of the processes applied locally, and the other applied globally: with X_1, X_2 , and κ_b as above, we

have

$$\begin{aligned}
 \mathbb{E} \sum_{x \in X_1 \cap W, y \in X_2 \cap W} \frac{\kappa_b(h - (y - x))}{\rho_2(y)} &= \int_W \int_W \kappa_b(h - (y - x)) c(y - x) \rho_1(x) \, dx \, dy \\
 &= \int_W \int_{W-x-h} \kappa_b(-z) c(h + z) \rho_1(x) \, dz \, dx \\
 &\simeq c(h) \int_{W \cap W_{-h}} \rho_1(x) \, dx
 \end{aligned}$$

for a small bandwidth $b > 0$, which suggests the partially-reweighted estimator

$$\hat{c}_{\text{partial}}(h) = \sum_{x \in X_1 \cap W, y \in X_2 \cap W} \frac{\kappa_b(h - (y - x))}{\rho_2(y) \int_{W \cap W_{-h}} \rho_1(x) \, dx},$$

207 provided $\int_{W \cap W_{-h}} \rho_1(x) \, dx > 0$. This estimator may be useful when ρ_2 is much easier to
 208 estimate than ρ_1 , e.g. when X_2 is homogeneous.

209 5. Sources of bias when ρ is estimated

210 All of the estimators of $K(t)$, $K_{12}(t)$, $g_0(h)$, and $g_1(r)$ discussed above are unbiased
 211 (at least when $t, \|h\|, r$ are sufficiently small) when the true intensity function ρ is used to
 212 compute the weight functions $\rho(x)\rho(y)$ in the local estimators or γ , γ^{iso} , γ_{12} , or γ_{12}^{iso} in the
 213 global estimators. However, in most applications ρ is not known, and must be replaced by
 214 an estimate. When the source of inhomogeneity is well understood, it is recommended to
 215 fit a model with an appropriate parametric intensity function and use it as the estimate, cf.
 216 Baddeley, Møller & Waagepetersen (2000) and Waagepetersen & Guan (2009).

217 In the absence of such a model, the most common alternative is a kernel estimator

$$\hat{\rho}(x) = \sum_{y \in X \cap W} \frac{\kappa_\sigma(y - x)}{w_W(x; y)} \tag{23}$$

where κ_σ is a symmetric kernel on \mathbb{R}^d with bandwidth $\sigma > 0$, and where $w_W(x; y)$ is an
 appropriate edge correction weight. We take the standard choice from Diggle (1985),

$$w_W(x; y) = \int_W \kappa_\sigma(u - x) \, du,$$

218 see also Van Lieshout (2012) (other types of edge corrections may depend on both x and y
 219 which is why we write $w_W(x; y)$ although the weight here only depends on x .)

220 In the following we discuss estimators for ρ and γ with particular focus on the
 221 implications of estimation bias when kernel estimators are used to replace the true γ or ρ
 222 in the global and local estimators.

223 5.1. Bias of local estimators with estimated ρ

224 We start by considering a single spatial point process X . For each point pair $x, y \in X$
 225 ($x \neq y$), the corresponding term in the local K - and pair correlation function estimators is
 226 normalized by the product $\rho(x)\rho(y)$. While an exact expression for the bias of the estimators
 227 with estimated ρ is not analytically tractable, we can understand major sources of bias by
 228 considering the expression $1/(\hat{\rho}(x)\hat{\rho}(y))$, which appears in each of the local estimators.

229 First, following Baddeley, Møller & Waagepetersen (2000), we note that $\hat{\rho}$ as defined in
 230 (23) is subject to bias when evaluated at the points of X , and that a ‘leave-one-out’ kernel
 231 estimator given by

$$\bar{\rho}(x) = \sum_{y \in (X \cap W) \setminus \{x\}} \frac{\kappa_{\sigma}(y-x)}{w_W(x; y)}, \quad x \in W, \quad (24)$$

232 is a better choice, with reduced bias in most cases.

233 Second, we note that

$$E(1/\bar{\rho}(x)) > 1/E(\bar{\rho}(x))$$

234 (if $E(1/\bar{\rho}(x))$ exists; in some cases it may be infinite). This follows from Jensen’s inequality,
 235 since $x \mapsto 1/x$ is strictly convex for $x > 0$. In addition, note that the leading contribution to
 236 $E(1/\bar{\rho}(x)) - 1/E(\bar{\rho}(x))$ is proportional to $\text{var}\bar{\rho}(x)$ (Liao & Berg 2019). This discrepancy
 237 leads to a strong positive bias of the local K - and pair correlation function estimators,
 238 especially at large $\|y-x\|$, where $1/\bar{\rho}(x)$ and $1/\bar{\rho}(y)$ are almost independent. This effect
 239 becomes more pronounced for smaller σ , since $\text{var}\bar{\rho}(x)$ typically increases as σ decreases.

240 Third, we note that for distinct points $x, y \in W$ that are close compared to the bandwidth
 241 σ , the covariance of $\bar{\rho}(x)$ and $\bar{\rho}(y)$ leads to bias. For the local (and global) estimators,
 242 we consider sums over distinct $x, y \in X \cap W$, which leads us to condition on $x, y \in X$ as
 243 follows (for details, see Coeurjolly, Møller & Waagepetersen 2017). By X conditioned on
 244 distinct points $x, y \in X$ with $\rho^{(2)}(x, y) > 0$, we mean that X is equal to $X_{xy} \cup \{x, y\}$ in
 245 distribution, where X_{xy} follows the second-order reduced Palm distribution of X at x, y :

$$\Pr(X \in F \mid x, y \in X) = \Pr(X_{xy} \cup \{x, y\} \in F).$$

Assuming X has n ’th order joint intensity functions $\rho^{(n)}$ for $n \leq 4$, X_{xy} has intensity
 function $\rho_{xy}(u) = \rho^{(3)}(x, y, u)/\rho^{(2)}(x, y)$ and second order joint intensity function

$\rho_{xy}^{(2)}(u, v) = \rho^{(4)}(x, y, u, v) / \rho^{(2)}(x, y)$. Now, for distinct $x, y \in W$ with $\rho^{(2)}(x, y) > 0$, neglecting the edge correction in (24) for simplicity, we obtain the following by the first and second-order Campbell's formulas for X_{xy} and using that κ_σ is symmetric:

$$\begin{aligned} \mathbb{E}[\bar{\rho}(x)\bar{\rho}(y) \mid x, y \in X \cap W] &= \mathbb{E} \left\{ \sum_{u \in (X_{xy} \cap W) \cup \{y\}} \kappa_\sigma(x-u) \sum_{v \in (X_{xy} \cap W) \cup \{x\}} \kappa_\sigma(y-v) \right\} \\ &= \mathbb{E} \sum_{u, v \in X_{xy} \cap W}^{\neq} \kappa_\sigma(x-u)\kappa_\sigma(y-u) + \mathbb{E} \sum_{u \in X_{xy} \cap W} \kappa_\sigma(x-u)\kappa_\sigma(y-u) \\ &\quad + \kappa_\sigma(x-y)\kappa_\sigma(y-x) \end{aligned} \quad (25)$$

$$\begin{aligned} &+ \kappa_\sigma(x-y)\mathbb{E} \sum_{v \in X_{xy} \cap W} \kappa_\sigma(y-v) + \kappa_\sigma(y-x)\mathbb{E} \sum_{u \in X_{xy} \cap W} \kappa_\sigma(x-u) \\ &= \int_W \int_W \kappa_\sigma(x-u)\kappa_\sigma(y-v) \frac{\rho^{(4)}(x, y, u, v)}{\rho^{(2)}(x, y)} du dv \end{aligned} \quad (26)$$

$$+ \int_W \kappa_\sigma(x-u)\kappa_\sigma(y-u) \frac{\rho^{(3)}(x, y, u)}{\rho^{(2)}(x, y)} du \quad (27)$$

$$+ \kappa_\sigma(x-y)^2 + \kappa_\sigma(x-y) \int_W \{\kappa_\sigma(x-u) + \kappa_\sigma(y-u)\} \frac{\rho^{(3)}(x, y, u)}{\rho^{(2)}(x, y)} du. \quad (28)$$

246 If X is a Poisson process, then X and X_{xy} are identically distributed, and so the term
247 in (26) simplifies to $\mathbb{E}\bar{\rho}(x)\mathbb{E}\bar{\rho}(y)$, which differs from $\rho(x)\rho(y)$ only by the inherent bias of
248 the kernel estimators. In general, the joint intensity $\rho^{(4)}(x, y, u, v)$ in the integrand of that
249 term represents the additional covariance of $\bar{\rho}(x)$ and $\bar{\rho}(y)$ due to interactions between the
250 points of the process, and induces further bias. For example, this bias will tend to overestimate
251 $\rho(x)\rho(y)$ for clustered processes, and lead to an underestimate of K , g_0 , and g_1 . The terms in
252 (27) and (28) are non-negative, and in particular the term in (27) can be large when x and y
253 are close together compared to σ . This positive bias leads to substantial negative bias at short
254 distances of the local estimators of K , g_0 , and g_1 .

255 In comparison, the conditional expectation $\mathbb{E}\{\hat{\rho}(x)\hat{\rho}(y) \mid x, y \in X\}$ would have
256 additional positive terms depending on $\kappa(0)$. In the two point process case, the relevant
257 conditional expectation $\mathbb{E}\{\bar{\rho}_1(x)\bar{\rho}_2(y) \mid x \in X_1, y \in X_2\}$ has an expression (of which we
258 omit the details) analogous to (27). However, since X_1 and X_2 are assumed to have a cross
259 pair correlation function, almost surely $u = v$ does not occur for $u \in X_1$ and $v \in X_2$, so no
260 term analogous to the second term in (27) occurs in $\mathbb{E}\{\bar{\rho}_1(x)\bar{\rho}_2(y) \mid x \in X_1, y \in X_2\}$. This
261 reduces the bias problem in the two point process case compared to the single point process
262 case.

263 For distinct $x, y \in W$ with $\rho^{(2)}(x, y) > 0$, a superior estimator for $\rho(x)\rho(y)$ might be
 264 given by

$$\overline{\rho(x)\rho(y)} = \sum_{u, v \in X \cap W \setminus \{x, y\}}^{\neq} \frac{\kappa(x-u)\kappa(y-v)}{w_W(x; u)w_W(y; v)}. \quad (29)$$

265 Then the terms in (27) and (28) are avoided, since

$$\mathbb{E}\{\overline{\rho(x)\rho(y)} \mid x, y \in X \cap W\} = \int_W \int_W \frac{\kappa(x-u)\kappa(y-v)}{w_W(x; u)w_W(y; v)} \frac{\rho^{(4)}(x, y, u, v)}{\rho^{(2)}(x, y)} du dv.$$

266 We do not investigate this idea further in the current work.

267 5.2. Bias of global estimators with estimated γ

268 Given the kernel estimate in (23) an immediate estimator of $\gamma(h)$, $h \in \mathbb{R}^d$, is

$$\hat{\gamma}(h) = \int_{W \cap W_{-h}} \hat{\rho}(z)\hat{\rho}(z+h) dz. \quad (30)$$

269 To understand properties of this estimator we evaluate its expected value. We start with the
 270 simplest case where h is a fixed vector in \mathbb{R}^d . This case is relevant for the global estimator
 271 of the pair correlation function. We return in the end of this section to the case where h is an
 272 observed difference $h = y - x$ for distinct $x, y \in X$, which occurs for the global estimator
 273 of the K -function.

Neglecting edge corrections for simplicity, we get

$$\mathbb{E}\hat{\gamma}(h) = \int_{W \cap W_{-h}} \int_W \kappa_\sigma(z-u)\rho(u) \int_W \kappa_\sigma(z+h-v)\rho(v)g_0(u-v) dv du dz \quad (31)$$

$$+ \int_{W \cap W_{-h}} \int_W \kappa_\sigma(z-u)\kappa_\sigma(z+h-u)\rho(u) du dz. \quad (32)$$

274 The two resulting terms are analogous to the terms in (26) and (27).

275 When $g_0 = 1$ as for a Poisson process, the term in the right hand side of (31) simplifies
 276 to

$$\int_{W \cap W_{-h}} \mathbb{E}\hat{\rho}(x)\mathbb{E}\hat{\rho}(x+h) dx.$$

277 This differs from $\gamma(h)$ due to the inherent bias of the kernel estimators which depends on
 278 the spatial structure of the intensity function: $\mathbb{E}\hat{\rho}(x) - \rho(x)$ becomes large when σ is large
 279 compared to the length scale of spatial variation of $\rho(x)$. On the other hand, when $g_0 \neq 1$,
 280 the term in the right hand side of (31) includes an additional bias due to the interaction
 281 between points. For example, this bias will tend to overestimate γ for clustered processes,
 282 and therefore lead to an underestimate of K or the pair correlation function. This interaction

283 bias is most pronounced when σ is small. In particular, as $\sigma \rightarrow 0$, this term approaches
 284 $g_0(y-x)\gamma(y-x)$, so that e.g. $E\hat{g}_{\text{global}}(h) \rightarrow 1$ for all $h \in \mathbb{R}^d$. However, in the typical case
 285 where the strength of pairwise interactions decreases with distance, increasing σ reduces bias
 286 due to interactions. Therefore, it is important to choose σ to be larger than the length-scale of
 287 interesting correlations.

288 The term in (32), though, is always positive when $h/2$ is in the support of κ_σ . We can
 289 avoid this term by using the following ‘leave-out’ estimator

$$\gamma(h) = \int_{W \cap W_{-h}} \sum_{u,v \in X \cap W}^{\neq} \frac{\kappa_\sigma(z-u)\kappa_\sigma(z+h-v)}{w(z;u)w(z+h;v)} dz, \quad (33)$$

290 where leave-out refers to omitting ‘diagonal terms’ $u = v$ in $\hat{\rho}(z)\hat{\rho}(z+h)$ (with $u, v \in$
 291 $X \cap W$). Similarly, when X is isotropic, an estimator of γ^{iso} can be defined in terms of
 292 $\bar{\gamma}$, as

$$\bar{\gamma}^{\text{iso}}(r) = r^{d-1} \int_{S^{d-1}} \bar{\gamma}(rs) d\nu_{d-1}(s). \quad (34)$$

For the global K -function estimators, γ is evaluated at $y-x$ for distinct $x, y \in X \cap W$.
 In this case the relevant expectation is $E\{\bar{\gamma}(y-x) \mid x, y \in X\}$. As in Section 5.1 we obtain
 this by considering the second-order reduced Palm distribution at distinct $x, y \in W$ with
 $\rho^{(2)}(x, y) > 0$, by assuming that X has n ’th order intensity functions $\rho^{(n)}$ for $n \leq 4$, and by
 neglecting the edge corrections for simplicity:

$$\begin{aligned} E\{\bar{\gamma}(y-x) \mid x, y \in X\} = & \\ & \int_{W \cap W_{-(y-x)}} \left(\int_W \int_W \frac{\rho^{(4)}(x, y, u, v)}{\rho^{(2)}(x, y)} \kappa_\sigma(z-u)\kappa_\sigma(z+(y-x)-v) du dv \right. \\ & + \kappa_\sigma(z-x)^2 + \kappa_\sigma(z-y)\kappa_\sigma(z+y-2x) \\ & + \int_W \frac{\rho^{(3)}(x, y, u)}{\rho^{(2)}(x, y)} [\{\kappa_\sigma(z-x) + \kappa_\sigma(z-y)\}\kappa_\sigma(z+(y-x)-u) \\ & \left. + \kappa_\sigma(z-u)\{\kappa_\sigma(z-x) + \kappa_\sigma(z+y-2x)\}] du \right) dz. \end{aligned}$$

293 Again, in case of a Poisson process, $\rho^{(4)}(x, y, u, v)/\rho^{(2)}(x, y) = \rho(u)\rho(v)$ and the first term
 294 is approximately $\gamma(y-x)$, subject to the subtleties discussed above. The other three terms
 295 are related to the terms with $u, v \in \{x, y\}$ of the double sum in (33), and yield a positive bias.
 296 We expect this bias to be small when σ is reasonably small, since the excess terms become
 297 negligible far from x and y , and the integral is over all of $W \cap W_{-h}$. The three terms could

298 be avoided by considering the further modified ‘leave-one pair-out’ estimator

$$\tilde{\gamma}(h; x, y) = \int_{W \cap W_{-h}} \sum_{\substack{\neq \\ u, v \in (X \cap W) \setminus \{x, y\}}} \frac{\kappa(z-u)\kappa(z+h-v)}{w(z; u)w(z+h; v)} dz, \quad \text{with } h = y - x,$$

299 but this depends on (x, y) not only through $h = y - x$ which precludes the use of
300 interpolation schemes as discussed in Section 5.3.

301 In case of two point processes we just use

$$\hat{\gamma}_{12}(h) = \int_{W \cap W_{-h}} \hat{\rho}_1(z)\hat{\rho}_2(z+h) dz$$

302 for kernel estimators $\hat{\rho}_1$ and $\hat{\rho}_2$, since in this case almost surely there are no diagonal terms
303 $u = v$ in $\hat{\rho}_1(z)\hat{\rho}_2(z+h)$ (with $u \in X_1$ and $v \in X_2$).

304 5.3. Computation of γ and γ^{iso}

305 We compute $\gamma(h)$ for a given intensity function ρ using a simple Monte Carlo
306 integration algorithm: we generate uniform random samples $U_i, i = 1, \dots, n$, on $W \cap W_{-h}$
307 and approximate $\gamma(h)$ by the unbiased Monte Carlo estimate

$$\gamma_{MC}(h) = \frac{|W \cap W_{-h}|}{n} \sum_{i=1}^n \rho(U_i)\rho(U_i+h). \quad (35)$$

308 To achieve a desired precision, we consider the standard error σ_{MC}/\sqrt{n} of $\gamma_{MC}(h)$ and
309 choose n so that the coefficient of variation becomes less than a selected threshold α :
310 $\sigma_{MC}/(\sqrt{n}\mu_{MC}) < \alpha$. For the simulation studies in Section 6, we used $\alpha = .001$ or $\alpha = .005$.
311 In practice, we wish to evaluate γ at many values of h . Thus it is convenient to generate a
312 single sequence of random samples $V_j, j = 1, \dots, n'$ on W , and for each h use a subsequence
313 $\{U_i^{(h)}\} = \{V_j \mid V_j \in W \cap W_{-h}\}$. We choose n' sufficiently large to produce the requisite
314 length of sub-sequence for each h .

315 For $\gamma^{\text{iso}}(r)$, we follow a similar approach, generating also random independent s_i
316 uniformly on $\{s \mid s \in \mathbb{S}^{d-1}, U_i + rs \in W\}$, and computing

$$\gamma_{MC}^{\text{iso}} = \frac{\int_{\mathbb{S}^{d-1}} |W \cap W_{-rs}| d\nu_{d-1}(s)}{s_d n} \sum_{i=1}^n \rho(U_i)\rho(U_i + rs_i). \quad (36)$$

317 The integral $\int_{\mathbb{S}^{d-1}} |W \cap W_{-rs}| d\nu_{d-1}(s)$ is easy to compute when W is a rectangular
318 window. As above, U_i and s_i are typically generated for each r as appropriate subsequences

319 of shared larger sequences V_j and t_j , respectively, sampled uniformly on W and \mathbb{S}^{d-1} ,
 320 respectively.

321 In practice ρ is replaced by an estimate. Then for the kernel-based leave-out estimator
 322 (33), $\rho(U_i)\rho(U_i + h)$ in (35) is replaced by

$$\sum_{u,v \in X \cap W}^{\neq} \frac{\kappa_\sigma(U_i - u)\kappa_\sigma(U_i + h - v)}{w(z; u)w(z + h; v)},$$

323 which is evaluated using a fast routine written in C. In a similar way, when X is isotropic and
 324 (34) is used, $\rho(U_i)\rho(U_i + rs_i)$ in (36) is replaced by a double sum.

325 Since γ and γ^{iso} are quite smooth, it is possible to interpolate them very accurately based
 326 on a moderate number of points h_j or r_j . This is especially helpful for γ^{iso} because it is one-
 327 dimensional. For the kernel-estimated $\bar{\gamma}^{\text{iso}}$ or $\hat{\gamma}^{\text{iso}}$, we find that linear interpolation based on
 328 sample spacing of $|r_{j+1} - r_j| < \sigma/10$ gives estimates within .01% of the true values. The
 329 interpolation scheme is especially helpful for the K -functions as the number of points grows
 330 large, in which case we must evaluate γ (or γ^{iso} in the isotropic case) at a very large number
 331 of pairs of points.

332 The proposed Monte Carlo computation becomes very slow when especially precise
 333 coefficient of variation α is desired, or when using kernel-based estimates with very small
 334 kernel bandwidth σ or large number of points N . For these cases, it may be beneficial to apply
 335 a variance reduction technique such as antithetic variables, or to consider an approximate
 336 convolution based on discrete Fourier transforms, with a kernel-based estimate of ρ , when
 337 desired, based on quadrat counts. When the side length of the quadrats is much less than σ ,
 338 we expect this method to produce accurate estimates of γ (or γ^{iso} in the isotropic case).

339 6. Simulation study

340 To compare global and local estimators for K and g , we simulated 100 point patterns
 341 on the unit square $W = [0, 1]^2$ for each of nine point process models obtained by combining
 342 three different types of point process interactions with four types of intensity functions. For
 343 plots of estimated K or g we simulated a further 1000 point patterns of the considered point
 344 process model.

345 More specifically we simulated stationary point processes of the types Poisson
 346 (no interaction), log-Gaussian Cox (LGCP – these are clustered/aggregated, see Møller,
 347 Syversveen & Waagepetersen 1998), and determinantal (DPP – these are regular/repulsive,
 348 see Lavancier, Møller & Rubak 2012), and subsequently subjected them to independent
 349 thinning to obtain various types of intensity functions. Note that independent thinnings

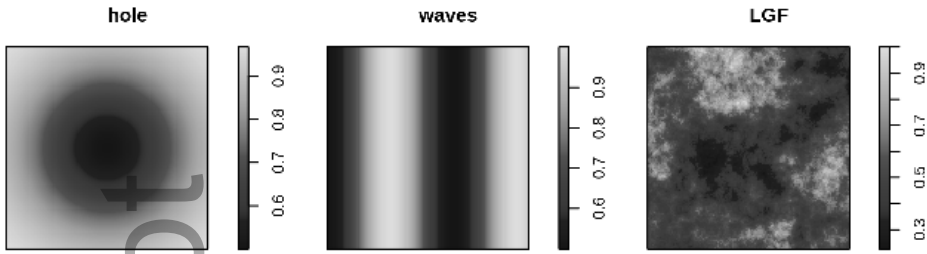


Figure 1. Plots of the ‘hole’, ‘waves’ and ‘LGF’ thinning profiles.

350 of stationary point processes are soirs (cf. Baddeley, Møller & Waagepetersen 2000). The
 351 intensities of the stationary point processes were adjusted to obtain on average 200 or 400
 352 points in the simulated point patterns (that is, after independent thinning).

353 For the Gaussian random field underlying the LGCP we used an exponential covariance
 354 function with unit variance and correlation scale 0.05 resulting in the isotropic pair correlation
 355 function

$$g_{\text{LGCP}}(r) = \exp\{\exp(-r/.05)\}.$$

356 For the DPP we used a Gaussian kernel with scaling parameter $\alpha = 0.02$ leading to

$$g_{\text{DPP}}(r) = 1 - \exp\{-2(r/.02)^2\}.$$

The intensity functions were of type constant (no thinning), ‘hole’, ‘waves’, or log-Gaussian random field (‘LGF’). Intensity functions of the ‘hole’ and ‘waves’ types were obtained by independent thinning using spatially varying retention probabilities

$$p_{\text{hole}}(x, y) = 1 - .5 \exp[-\{(x - .5)^2 + (y - .5)^2\} /.18],$$

$$p_{\text{waves}}(x, y) = 1 - .5 \cos^2(5x),$$

$$p_{\text{LGF}}(x, y) = \lambda(x, y) / \sup_{(u,v) \in W} \lambda(u, v),$$

357 for $(x, y) \in [0, 1]^2$. In case of ‘LGF’, $\log \lambda$ was generated as a realisation of a Gaussian
 358 random field with exponential covariance function, with variance .1 and correlation scale .3.
 359 The resulting ‘LGF’ retention probability surface is much less smooth than for ‘hole’ and
 360 ‘waves’ but similar to ‘hole’ and ‘waves’ in terms of intensity contrast and spatial separation
 361 of high-intensity and low-intensity regions. The surfaces of retention probabilities are shown
 362 in Figure 1.

363 Simulations were carried out and analyzed using the R package `spatstat`, and a
 364 new package `globalKinhom` that implements the global K - and pair correlation function
 365 estimators using Monte-Carlo estimates of γ as described in Section 5.3 (Baddeley, Rubak
 366 & Turner 2015; ?). In most cases we set the precision of the Monte-Carlo estimates to
 367 $\alpha = .005$. When probability intervals and root integrated mean square error (RIMSE) values
 368 are shown, we use $\alpha = .001$ instead, where the more precise calculation produced slightly
 369 smaller RIMSE values. We also tested smaller values of α in a few particular cases, and did
 370 not observe any reduction in RIMSE values below $\alpha = .001$. We do not show simulation
 371 results for all scenarios since in many cases the different scenarios led to qualitatively similar
 372 conclusions.

373 To investigate our cross K and cross pair correlation function estimators we generated
 374 simulations from a bivariate LGCP detailed in Section 6.2.

375 6.1. Estimation of K and pair correlation functions

376 We initially compare the bias of global and local estimators of the K -function using
 377 in both cases kernel estimators of the intensity function obtained with a Gaussian kernel
 378 with bandwidth σ chosen by the method of Cronie & van Lieshout (2018), as implemented
 379 in the `spatstat` procedure `bw.CvL` (CvL for convenience in the following). The selected
 380 bandwidths vary around .05 (see third column in Table 1), with slightly larger bandwidths for
 381 LGCP than for Poisson and DPP. For the global estimator we consider the isotropic estimator
 382 (5), since the pair correlation functions of the point processes tested here are all isotropic, as
 383 in the setting of Section 3.1.1, and the estimation of γ^{iso} is less computationally intensive than
 384 that of γ . We consider both the estimator (30) and the leave-out estimator (33) of the function
 385 γ . Similarly we also consider the local estimator using either the original kernel estimator
 386 (23) or the leave-out estimator (24) suggested in Baddeley, Møller & Waagepetersen (2000).

387 For better visualisation of the simulation results we transform the K -function estimators
 388 into estimators of the so-called $\{L(r) - r\}$ -function via the one-to-one transformation

$$L(r) - r = \sqrt{K(r)/\pi} - r.$$

389 We only show results in case of the waves intensity function with on average 400 simulated
 390 points, since the results for the other intensity functions and with on average 200 simulated
 391 points give the same qualitative picture.

392 Figure 2 shows averages of the simulated estimates and it is obvious that the global
 393 estimators are much less biased than the local estimators. It is clearly advantageous to use the
 394 leave-out versions for the global estimator. The leave-out approach is also advantageous for
 395 the local estimator, at least for small distances r . The biases of the leave-out local estimator

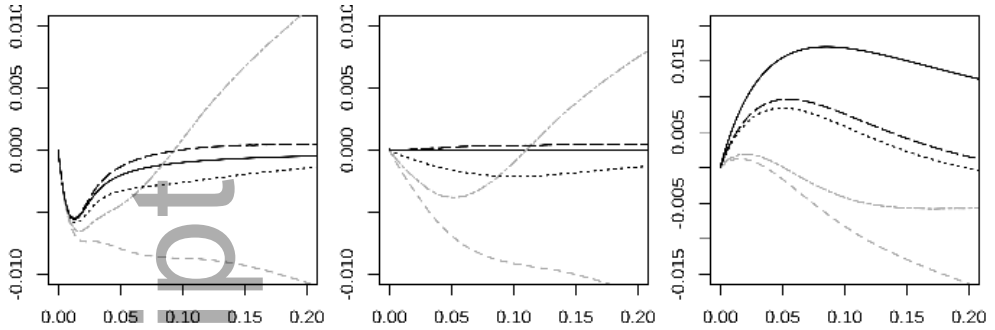


Figure 2. Averages of estimates of $L(r) - r$ obtained from simulations in case of the waves intensity function with 400 simulated points on average. Left to right: DPP, Poisson, LGCP. The estimates are obtained using $\hat{K}_{\text{global}}^{\text{iso}}$ with or without the leave-out approach (-----, , respectively) or \hat{K}_{local} with or without the leave-out approach (-----, -----, respectively) for kernel estimation of γ or the intensity function. True values of $L(r) - r$ are shown for comparison (———).

Table 1. Mean (\pm st. dev.) of CVL and LCV bandwidths, for each type of spatial point process we considered. The expected number of points for each listed process is 400.

Interaction type	Intensity function	σ_{CVL}	σ_{LCV}
DPP	constant	0.046 (0.005)	0.63 (0.15)
	hole	0.045 (0.004)	0.33 (0.22)
	waves	0.048 (0.004)	0.28 (0.25)
	LGF	0.047 (0.005)	0.22 (0.16)
Poisson	constant	0.047 (0.006)	0.59 (0.21)
	hole	0.048 (0.007)	0.29 (0.23)
	waves	0.050 (0.006)	0.14 (0.11)
	LGF	0.050 (0.006)	0.17 (0.13)
LGCP	constant	0.066 (0.009)	0.040 (0.007)
	hole	0.064 (0.012)	0.044 (0.008)
	waves	0.071 (0.011)	0.042 (0.008)
	LGF	0.066 (0.011)	0.042 (0.007)

396 are as discussed in Section 5.1: strong negative bias at short distances due to the covariance
 397 of $\bar{\rho}(x)$ and $\bar{\rho}(y)$, and strong positive bias at large distances due to Jensen's inequality
 398 $E(1/\bar{\rho}(x)) > 1/E(\bar{\rho}(x))$. The leave-out global estimator appears to be close to unbiased in
 399 case of DPP and Poisson but is too small on average in case of LGCP.

400 There exist a number of alternatives to the CVL approach to choosing the bandwidth
 401 for the kernel estimation. We therefore also investigate bias in the case where the bandwidth
 402 is selected using the likelihood cross validation (LCV) method implemented in the `spatstat`
 403 procedure `bw.ppl`. Results regarding the LCV selected bandwidths are summarised in the
 404 fourth column of Table 1. Comparison of the CVL and LCV results in Table 1 shows that the

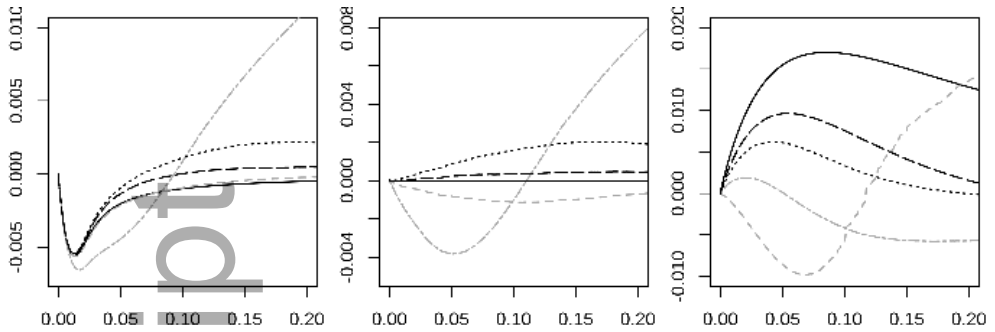


Figure 3. Averages of estimates of $L(r) - r$ obtained from simulations in case of the waves intensity function with 400 simulated points on average. Left to right: DPP, Poisson, LGCP. The estimates are obtained using the global (----- CVL, LCV) or local (——— CVL, - - - - - LCV) estimators of the K -function with either CVL or LCV for selecting the bandwidth (in all cases the leave-out approach is used). True values of $L(r) - r$ are shown for comparison (———).

405 LCV approach tends to select considerably larger bandwidths σ than the CVL method for the
 406 DPP and Poisson process, and somewhat smaller σ for the LGCP.

407 Figure 3 compares averages of the global and local estimators using either of the two
 408 approaches to bandwidth selection and with leave-out in all cases. Again we show only results
 409 for the waves intensity function and expected number of points equal to 400. The bias of the
 410 estimators is quite sensitive to the choice of bandwidth selection method. In case of DPP and
 411 Poisson, the global estimator using CVL and the local estimator using LCV perform similarly
 412 with the global estimator a bit more biased than the local for DPP and vice versa for Poisson.
 413 The global estimator performs slightly worse when combined with LCV than with CVL,
 414 likely due to the inherent biases of the kernel estimator $\bar{\rho}$, which become more pronounced as
 415 σ increases. The local estimator with CVL is strongly biased for almost all r considered. The
 416 improved performance with LCV is likely due to the reduced variances and covariances for
 417 $\bar{\rho}$ when a larger bandwidth is used. This also explains the strong bias of the local estimator
 418 with LCV for the LGCP, since σ_{LCV} is typically smaller than σ_{CVL} in that case. The global
 419 estimator for the LGCP has the smallest bias with the CVL method and has much less bias
 420 than the local estimator regardless of whether CVL or LCV is used. It is not surprising that
 421 the LGCP is the most challenging case for both the global and local estimators, since the
 422 random aggregation of the LGCP tends to be entangled with the variation in the intensity
 423 function.

424 We finally compare the sampling variability of the leave-out global estimator using
 425 CVL and the leave-out local estimator using LCV. Figure 4 shows 95% pointwise probability
 426 intervals and averages for the two estimators, again with 400 simulated points on average and
 427 the ‘waves’ intensity function, and Table 2 gives root integrated mean square error (RIMSE)

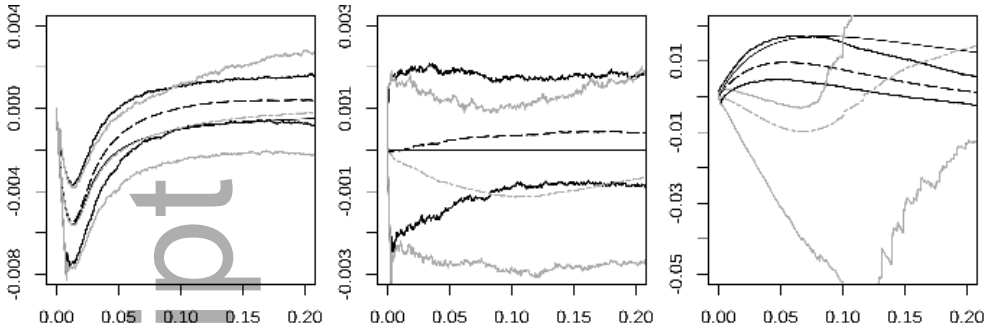


Figure 4. Averages and 95% pointwise probability intervals for estimates of $L(r) - r$ in case of the waves intensity function with 400 simulated points on average. Left to right: DPP, Poisson, LGCP. The estimators used are the leave-out global estimator using CVL (-----) and the leave-out local estimator using LCV. (-----), with pointwise probability intervals shown in like shade. True values of $L(r) - r$ are also shown (———).

428 values for the K -function estimators applied to each process, for each combination of CVL or
 429 LCV with the local or global leave-out estimator. Figure 4 indicates that the global estimator
 430 has smaller variance than the local estimator. This should also result in smaller mean square
 431 error for Poisson and LGCP where the bias is also smallest for the global estimator. For DPP
 432 the picture is not completely clear regarding mean square error since in this case the global
 433 estimator has larger bias than the local estimator. Table 2 gives more insight where a first
 434 observation is that the leave-out local estimator is very sensitive to the choice of bandwidth
 435 selection method with LCV performing much better than CVL for DPP and Poisson and vice
 436 versa for LGCP. The leave-out global estimator is much less sensitive to choice of bandwidth
 437 selection method. Best results in terms of RIMSE are obtained with the leave-out global
 438 estimator combined with CVL.

439 Figure 5 shows averages of leave-out global and local estimators of the isotropic pair
 440 correlation function using either CVL or LCV in case of the wave intensity with 400 points on
 441 average. Once again, local estimators are most strongly biased with the bandwidth selection
 442 method that produces the smaller bandwidth: CVL for the DPP and Poisson processes, and
 443 LCV for the LGCP. The bias is small to moderate for the global estimators with largest bias
 444 in case of LGCP. For the DPP and Poisson case positive bias of the local and global estimator
 445 occurs for very small distances.

446 6.2. Estimation of cross K and cross pair correlation functions

447 To investigate the cross K and cross pair correlation function estimators, we simulated
 448 100 bivariate point patterns for each model of a bivariate point process (X_1, X_2) , where
 449 either X_1 and X_2 are independent or display segregation or co-clustering. Processes that

Table 2. RIMSE $\times 10^2$ of local and global K -function estimators with CVL and LCV bandwidths.

Interaction type	Intensity function	\hat{K}_{local}		\hat{K}_{global}	
		CVL	LCV	CVL	LCV
DPP	flat	0.59	0.069	0.029	0.060
	hole	0.64	0.107	0.031	0.128
	waves	0.60	0.052	0.049	0.121
	LGF	0.59	0.060	0.050	0.110
Poisson	flat	0.45	0.083	0.028	0.069
	hole	0.45	0.120	0.034	0.103
	waves	0.40	0.061	0.037	0.093
	LGF	0.37	0.087	0.050	0.089
LGCP	flat	0.89	0.999	0.573	0.628
	hole	0.87	1.554	0.576	0.636
	waves	0.89	1.146	0.528	0.613
	LGF	0.90	1.506	0.542	0.625

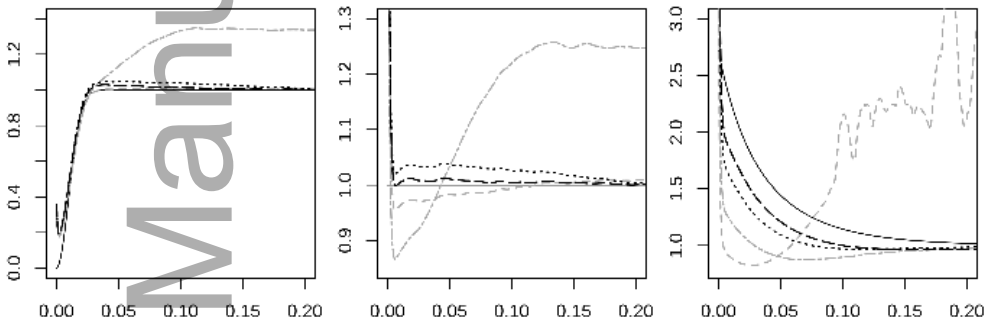


Figure 5. Averages of estimates of $g_1(r)$ obtained from simulations in case of the waves intensity function with 400 simulated points on average. Left to right: DPP, Poisson, LGCP. The estimates are obtained using the global (----- CVL, LCV) or local (..... CVL, ----- LCV) estimators of the pair correlation function with either CVL or LCV bandwidth selection. (In each case, the leave-out approach is used.) True values of $g(r)$ are shown for comparison (——).

450 were chosen for plotting were simulated an additional 1000 times. Inhomogeneous intensity
 451 functions were subsequently obtained using independent thinning of stationary bivariate point
 452 processes, where the two point processes have the same intensity, and the constant, ‘hole’,
 453 and ‘waves’ retention probabilities p as described in connection to Figure 1 were used. This
 454 implies $\rho_1(x) = \rho_2(x)$ for $x \in [0, 1]^2$ (we did not investigate any scenarios where $\rho_1 \neq \rho_2$).

455 In the case of independence, X_1 and X_2 are independent Poisson processes. For the
 456 dependent cases, we considered a bivariate LGCP. Specifically, for $i = 1, 2$, X_i has random
 457 intensity function

$$\Lambda_i(u) = p(u) \exp\{\mu_i + \alpha_i Y(u) + \beta U_i(u)\}, \quad i = 1, 2,$$

458 where Y , U_1 , and U_2 are independent zero-mean unit-variance Gaussian random fields with
 459 isotropic exponential correlation functions given by $\exp(-r/\phi)$ and $\exp(-r/\psi_i)$ ($r \geq 0$),
 460 $i = 1, 2$, respectively, and where $\mu_i \in \mathbb{R}$, $\alpha_i \in \mathbb{R}$, and $\beta > 0$ are parameters. This means
 461 that X_1 and X_2 conditioned on (Λ_1, Λ_2) are independent Poisson processes with intensity
 462 functions Λ_1 and Λ_2 , respectively. The (cross) pair correlation functions for this class of
 463 bivariate LGCP are isotropic, where the pair correlation function of X_i is given by

$$g_i^{\text{iso}}(r) = \exp\{\alpha_i^2 \exp(-r/\phi) + \beta \exp(-r/\psi_i)\}, \quad i = 1, 2,$$

464 and the cross pair correlation function of (X_1, X_2) is given by

$$c^{\text{iso}}(r) = \exp\{\alpha_1 \alpha_2 \exp(-r/\phi)\}.$$

465 Note that $c^{\text{iso}} < 1$ if $\alpha_1 \alpha_2 < 0$ (the case of segregation between X_1 and X_2), and $c^{\text{iso}} > 1$
 466 if $\alpha_1 \alpha_2 > 0$ (the case of co-clustering between X_1 and X_2). For the segregated processes,
 467 we chose $\alpha_1 = -\alpha_2 = 1$, $\phi = .03$, $\beta = .25$, $\psi_1 = .02$, and $\psi_2 = .01$. For the co-clustered
 468 case, we used $\alpha_1 = \alpha_2 = 1$ and the other parameters as for the segregated case. With these
 469 choices, the cross correlation functions become

$$c_{\text{segr}}^{\text{iso}}(r) = \exp\{-\exp(-r/.03)\}$$

470 for the segregation case and

$$c_{\text{cluster}}^{\text{iso}}(r) = \exp\{\exp(-r/.03)\}$$

471 for the co-clustered case. Finally, we adjusted μ_1 and μ_2 so that the expected number of points
 472 after independent thinning is 200 or 400.

473 For the global estimator of K_{12} , we consider again the isotropic estimator (13), since
 474 in each case the cross pair correlation function is isotropic, and estimation of $\gamma_{12}^{\text{iso}}(r)$ is
 475 less computationally intensive than that of $\gamma_{12}(h)$. For the local estimator we consider the
 476 estimator (11), with ρ_i estimated by the leave-out kernel estimator $\bar{\rho}$ from (24). Similar to the
 477 $\{L(r) - r\}$ -function used above, we transform the K_{12} -function estimators into estimators
 478 of the $\{L_{12}(r) - r\}$ -function, by the one-to-one transformation

$$L_{12}(r) - r = \sqrt{K_{12}(r)/\pi} - r.$$

479 Figure 6 shows averages of estimators of $L_{12}(r) - r$ in case of the waves intensity and
 480 expected number of points equal to 400. The bandwidth is selected using the CVL or LCV
 481 procedure applied to X_1 . Table 3 gives selected bandwidth values for the pairs of spatial

Table 3. Mean (\pm st. dev.) of CVL and LCV selected bandwidths for the simulated two point process cases. Expected number of points is 400 for each listed process.

Interaction type	Intensity function	σ_{CVL}	σ_{LCV}
Segregated	constant	0.063 (0.008)	0.038 (0.006)
	hole	0.062 (0.009)	0.039 (0.008)
	waves	0.064 (0.010)	0.040 (0.008)
Poisson	constant	0.048 (0.006)	0.60 (0.19)
	hole	0.048 (0.006)	0.28 (0.22)
	waves	0.051 (0.006)	0.19 (0.20)
Co-clustered	constant	0.062 (0.008)	0.040 (0.008)
	hole	0.060 (0.009)	0.040 (0.007)
	waves	0.064 (0.011)	0.040 (0.009)

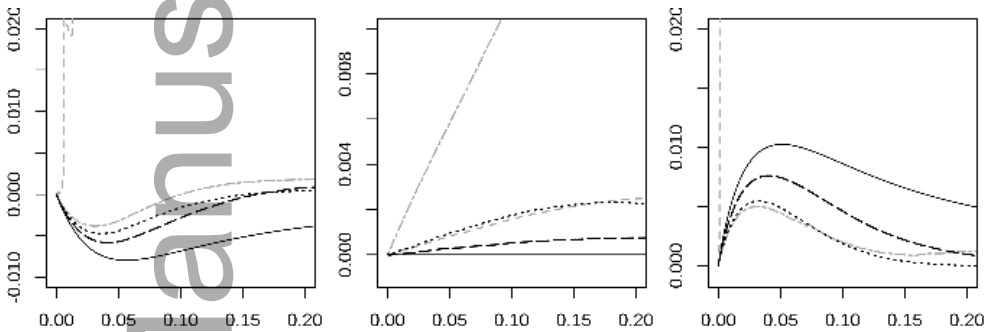


Figure 6. Averages of estimates of cross- $L(r) - r$ in case of the waves intensity function with 400 simulated points on average. Left to right: segregation, independence, co-clustering. The estimators used are the standard global (--- CVL, LCV) and local (— CVL, - - - LCV) leave-out estimators of K_{12} combined with the CVL and LCV methods for the bandwidth selection. True values of $L_{12}(r) - r$ are shown for comparison (—).

482 point processes we considered. The results are similar to the one point process case. Both the
 483 segregated and co-clustered LGCP typically yield $\sigma_{LCV} < \sigma_{CVL}$ while the opposite is true
 484 for the Poisson case. Further, the local estimators are strongly biased, and the bias increases as
 485 the bandwidth σ decreases: in the case of segregation and co-clustering, the local estimators
 486 are better with CVL, while LCV is better in the case of independence. Note also that the
 487 negative bias that is observed at small distances r for \hat{K}_{local} is absent here as predicted in the
 488 discussion in Section 5.1. The bias for the global estimator with CVL is smaller than for the
 489 best local estimators in each case.

490 To compare sampling variability for the estimators of the cross K -function, we show
 491 pointwise 95% probability intervals for estimated $L_{12}(r) - r$ in Figure 7. The bandwidth
 492 selection method that produces the least bias in each case is shown. Table 4 shows root
 493 integrated mean square error of the estimators of K_{12} . In every case, the best global estimator

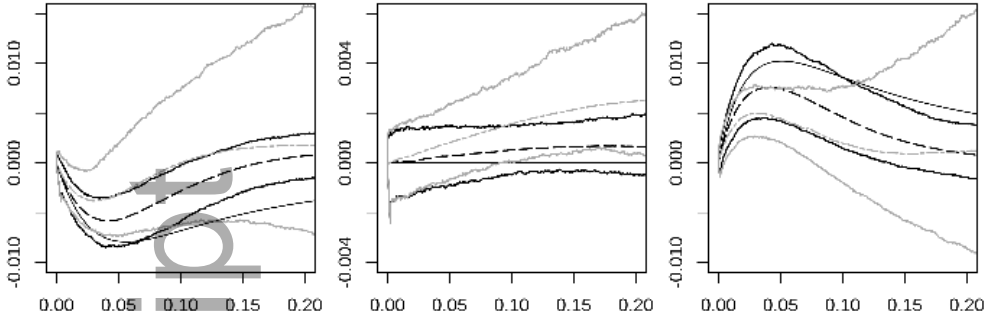


Figure 7. Averages and 95% pointwise probability intervals for estimates of $L_{12}(r) - r$ in case of the waves intensity function with 400 simulated points on average. Left to right: segregation, independence, co-clustering. The estimators used are the leave-out global estimator (-----) and the leave-out local estimator (-----), with pointwise probability intervals shown in like shade. In each case, the bandwidth selection method was chosen to produce the least bias: LCV for the local estimator on the independent process, and CVL for all the other cases. True values of $L_{12}(r) - r$ are also shown (——).

Table 4. Root integrated mean squared errors $\times 10^2$ of local and global K_{12} -function estimators with CVL and LCV bandwidths.

Interaction type	Intensity function	$\hat{K}_{12,\text{local}}$		$\hat{K}_{12,\text{global}}$	
		CVL	LCV	CVL	LCV
Segregated	flat	0.65	390.125	0.161	0.181
	hole	0.69	4.574	0.171	0.185
	waves	0.64	270.633	0.208	0.201
Independent	flat	1.03	0.066	0.024	0.049
	hole	1.09	0.112	0.026	0.109
	waves	0.95	0.191	0.037	0.104
Co-clustered	flat	0.92	18.783	0.234	0.262
	hole	0.97	3.510	0.239	0.265
	waves	0.92	5.238	0.195	0.244

494 has smaller integrated mean square error than the best local estimator, as expected from the
 495 considerations of Section 3.1.2.

496 For the estimation of the cross pair correlation functions, the conclusions are similar to
 497 those for the cross K -functions, see Figure 8. The average of the global estimator is quite
 498 close to the true cross pair correlation function, while the local estimator is strongly biased.
 499 Note that $\hat{c}_{\text{local}}^{\text{LCV}}$ is missing for the segregated and co-clustered processes, because the average
 500 values of that estimator were extremely large.

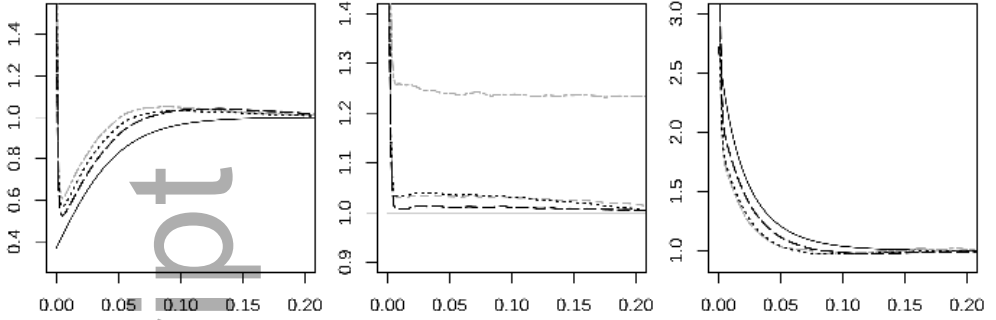


Figure 8. Averages of estimates of $c(r)$ in case of the waves intensity function with 400 simulated points on average. Left to right: segregation, independence, co-clustering. The estimators used are the leave-out global (----- CVL, LCV) and local (----- CVL, LCV) estimators combined with the CVL and LCV methods for bandwidth selection. True values of $L_{12}(r) - r$ are shown for comparison (——).

501 6.3. Estimation of K -function using a parametric estimate for ρ

502 Returning to the setting of a single point process X as in the beginning of Section 6,
 503 we also consider the case of a parametric model where the intensity $\alpha > 0$ of the underlying
 504 stationary point process (that is, before thinning) is unknown but the retention probability
 505 function p that was used to thin the point process is known. Then a simple parametric
 506 estimator for ρ is given by

$$\hat{\rho}_p(x) = Np(x) / \int_W p(x) dx, \quad (37)$$

507 where N is the number of points in $X \cap W$. We apply this intensity estimator to \hat{K}_{local} and
 508 \hat{K}_{global} for 1000 realisations of each interaction type, with the ‘waves’ intensity function and
 509 expected number of points equal to 400. In addition, we generate 1000 simulations for each
 510 interaction type with a new thinning profile, ‘deep waves’, given by

$$p_{\text{deep}}(x, y) = 1 - .9 \cos^2(5x), \quad (x, y) \in [0, 1]^2.$$

511 The deep waves profile is similar to the waves profile, but with much more extreme intensity
 512 variations.

513 Pointwise probability intervals for estimates of $L(r) - r$ are shown in Figure 9, and root
 514 integrated mean square error for estimates of K are given in Table 5. We observe that in all
 515 cases the error of the global estimator is comparable to or better than the corresponding local
 516 estimator. For the ‘waves’ intensity function, the difference is small. Both estimators have
 517 larger error when applied to the patterns with the ‘deep waves’ intensity function. However,

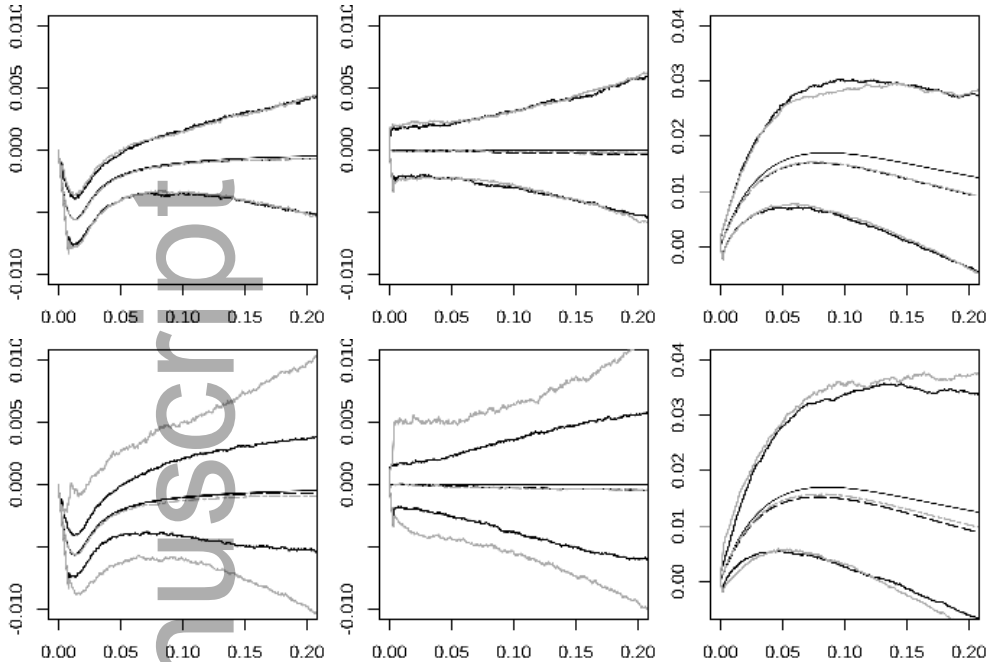


Figure 9. Averages and 95% pointwise probability intervals for estimates of $L(r) - r$ in case of the ‘waves’ (top row) or ‘deep waves’ (bottom row) intensity function with 400 simulated points on average. Left to right: DPP, Poisson, LGCP. The estimators used are the global (-----) and local (——) estimators using the parametric intensity estimator (37). Pointwise probability intervals are shown in like shade. True values of $L(r) - r$ are also shown (——).

518 the performance of the local estimator degrades much more strongly, reflecting the fact that
 519 regions of low intensity are weighted more heavily in \hat{K}_{local} than in \hat{K}_{global} , as discussed in
 520 Section 3.1.2. The LGCP yielded the largest errors with the parametric intensity estimates,
 521 similar to our observations with the kernel-based intensity estimates. We also note that for
 522 the DPP and the Poisson process, using the parametric estimates for the ‘waves’ intensity
 523 function results in higher integrated mean square error than for the kernel-based estimates
 524 (Table 2). We believe this is because the kernel-based estimates of ρ are adapted to the
 525 random local fluctuations of the point processes, similar to how homogeneous K -function
 526 estimates have lower variance when using estimated intensity than true intensity. However,
 527 for the LGCP, best results are obtained with the parametric estimates, which presumably are
 528 less prone to confounding of random clustering with variations in the intensity function.

7. Extensions

529
 530 The same sort of analysis as in Sections 3–4 could be applied to point processes defined
 531 on a non-empty manifold on which a group acts transitively (a so-called homogeneous space),

Table 5. Root integrated mean squared errors $\times 10^2$ of local and global K -function estimators with parametric intensity estimator, applied to point processes with intensity function ‘waves’ or ‘deep waves’.

Interaction type	Intensity function	\hat{K}_{local}	\hat{K}_{global}
DPP	waves	.111	.102
	deep waves	.227	.103
Poisson	waves	.132	.122
	deep waves	.239	.133
LGCP	waves	.416	.417
	deep waves	.601	.516

532 where the space is equipped with a reference measure which is invariant under the group
 533 action. In this paper, the space was \mathbb{R}^d , the group action was given by translations, and
 534 the reference measure was Lebesgue measure. For example, instead we could consider the
 535 space to be a d -dimensional sphere, with the group action given by rotations and where the
 536 reference measure is the corresponding d -dimensional surface measure. Then the global and
 537 local estimators considered in this paper are simply modified to the case of the sphere by
 538 replacing Lebesgue with surface measure and using appropriate edge correction factors as
 539 defined in Lawrence et al. (2016). Similarly, our global estimators could also be extended
 540 to the case of spatio-temporal point processes, as in Gabriel & Diggle (2009) and Møller &
 541 Ghorbani (2012).

542 8. Conclusion

543 According to our simulation studies, our new global estimators outperform the existing
 544 local estimators in terms of bias and mean integrated squared error when kernel or parametric
 545 estimators are used for the intensity function. The kernel intensity function estimators
 546 depend strongly on the choice of bandwidth and we considered two different data-driven
 547 approaches, CVL and LCV, to bandwidth selection. In our simulation studies the two
 548 approaches gave similar selected bandwidths in the LGCP case but very different results
 549 in case of Poisson and DPP. This has a considerable impact on the K - and pair correlation
 550 function estimators but the global estimators appear to be much less sensitive to the choice of
 551 bandwidth selection method than the local estimators. The simulation studies with parametric
 552 estimates of the intensity function, along with the theory of Section 3.1.2, indicate that the
 553 global estimators are also much less sensitive to regions of especially low intensity. The
 554 improved statistical efficiency comes at a considerable extra computational cost. Therefore,
 555 we especially recommend the global estimators for situations where intensity variations are
 556 large and where computational speed is not a primary concern.

557

References

- 558 BADDELEY, A., RUBAK, E. & TURNER, R. (2015). *Spatial Point Patterns: Methodology and Applications*
559 *with R*. London: Chapman & Hall/CRC Press.
- 560 BADDELEY, A.J., MØLLER, J. & WAAGEPETERSEN, R. (2000). Non- and semi-parametric estimation of
561 interaction in inhomogeneous point patterns. *Statistica Neerlandica* **54**, 329–350.
- 562 CHIU, S., STOYAN, D., KENDALL, W. & MECKE, J. (2013). *Stochastic Geometry and Its Applications*.
563 Wiley Series in Probability and Statistics, Chichester: John Wiley & Sons, Ltd.
- 564 COEURJOLLY, J.F., MØLLER, J. & WAAGEPETERSEN, R. (2017). A Tutorial on Palm Distributions for
565 Spatial Point Processes. *International Statistical Review* **85**, 404–420.
- 566 CRONIE, O. & VAN LIESHOUT, M.N.M. (2018). A non-model-based approach to bandwidth selection for
567 kernel estimators of spatial intensity functions. *Biometrika* **105**, 455–462.
- 568 DIGGLE, P. (1985). A kernel method for smoothing point process data. *Journal of the Royal Statistical*
569 *Society: Series C (Applied Statistics)* **34**, 138–147.
- 570 GABRIEL, E. & DIGGLE, P.J. (2009). Second-order analysis of inhomogeneous spatio-temporal point
571 process data. *Statistica Neerlandica* **63**, 43–51.
- 572 ILLIAN, J., PENTTINEN, A., STOYAN, H. & STOYAN, D. (2008). *Statistical Analysis and Modelling of*
573 *Spatial Point Patterns*. Statistics in Practice, Chichester: John Wiley & Sons, Ltd.
- 574 LANG, G. & MARCON, E. (2013). Testing randomness of spatial point patterns with the Ripley statistic.
575 *ESAIM: Probability and Statistics* **17**, 767–788.
- 576 LAVANCIER, F., MØLLER, J. & RUBAK, E. (2012). Determinantal point process models and statistical
577 inference. *Journal of the Royal Statistical Society: Series B (Statistical Methodology)* **77**.
- 578 LAWRENCE, T., BADDELEY, A.J., MILNE, R. & NAIR, G. (2016). Point pattern analysis on a region of a
579 sphere. *Stat* **5**, 144–157.
- 580 LIAO, J.G. & BERG, A. (2019). Sharpening Jensen’s inequality. *The American Statistician* **73**, 278–281.
- 581 MØLLER, J. & GHORBANI, M. (2012). Aspects of second-order analysis of structured inhomogeneous
582 spatio-temporal point processes. *Statistica Neerlandica* **66**, 472–491.
- 583 MØLLER, J. & RUBAK, E. (2016). Functional summary statistics for point processes on the sphere with an
584 application to determinantal point processes. *Spatial Statistics* **18**, 4 – 23.
- 585 MØLLER, J., SYVERSVEEN, A.R. & WAAGEPETERSEN, R.P. (1998). Log Gaussian Cox processes.
586 *Scandinavian Journal of Statistics* **25**, 451–482.
- 587 MØLLER, J. & WAAGEPETERSEN, R.P. (2004). *Statistical Inference and Simulation for Spatial Point*
588 *Processes*. Boca Raton: Chapman & Hall/CRC Press.
- 589 MØLLER, J. & WAAGEPETERSEN, R.P. (2007). Modern statistics for spatial point processes. *Scandinavian*
590 *Journal of Statistics* **34**, 643–711.
- 591 OHSER, J. & STOYAN, D. (1981). On the second-order and orientation analysis of planar stationary point
592 processes. *Biometrical Journal* **23**, 523–533.
- 593 RIPLEY, B.D. (1988). *Statistical Inference for Spatial Processes*. Cambridge: Cambridge University Press.
- 594 STONE, M.B., SHELBY, S.A., NÚÑEZ, M.F., WISSER, K. & VEATCH, S.L. (2017). Protein sorting by lipid
595 phase-like domains supports emergent signaling function in B lymphocyte plasma membranes. *eLife* **6**,
596 e19891.
- 597 VAN LIESHOUT, M.N.M. (2011). A J -function for inhomogeneous point processes. *Statistica Neerlandica*
598 **65**, 183–201.
- 599 VAN LIESHOUT, M.N.M. (2012). On estimation of the intensity function of a point process. *Methodology*
600 *and Computing in Applied Probability* **14**, 567–578.
- 601 WAAGEPETERSEN, R. & GUAN, Y. (2009). Two-step estimation for inhomogeneous spatial point processes.
602 *Journal of the Royal Statistical Society: Series B (Statistical Methodology)* **71**, 685–702.